Transition dynamics and metastable states during premelting and freezing of ice surfaces

Shifan Cui[1,*] and Haoxiang Chen[2]

[1]*International Center for Quantum Materials, School of Physics, Peking University, 209 Chengfu Road, Haidian District, Beijing 100871, China*

[2]*School of Physics, Peking University, 209 Chengfu Road, Haidian District, Beijing 100871, China*

(Received 18 November 2022; revised 9 June 2023; accepted 6 July 2023; published 21 July 2023)

The premelting of ice is well known, but little is known about how the premelted and solid surfaces convert to each other. In this work, the transition dynamics between two phases are revealed with large-scale molecular dynamics simulations. Supercooling and superheating states exist in the transition, and are overcome by nucleation-like processes. The natural inhomogeneity of ice surfaces enhances nuclei formation, while it only accelerates premelting but not freezing. Furthermore, the complete freezing of ice surfaces may be hindered by the stacking order mismatch between nuclei. This work points out the importance of metastable states in premelting, and the necessity of a large system scale in describing its transition process.

DOI: 10.1103/PhysRevB.108.045413

I. INTRODUCTION

The premelting of ice, namely the existence of a quasiliquid layer (QLL) on the ice surface below the melting point, has been recognized for more than 170 years since Faraday's experiment in 1850 [1]. Due to its important role in various environmental processes [2–5] and the rich physics inside [6–8], premelting has been of research interest for decades [8]. There are considerable studies about the onset of premelting [9–15], the thickness [16–21] and structure [21–27] of QLL, how it behaves during growth or evaporation [28–32], and its interaction with external solvents [33–38] or confinements [39–43].

Despite the progress, there are still several questions about premelting that remain unsolved. There are large discrepancies within the premelting onsets and QLL thicknesses reported in the literature [8,44], and it is doubtful if a particular "transition temperature" exists [45]. Droplets are found on the QLL at certain ranges of temperature and vapor pressure [30], but the microscopic mechanism of how they emerge and disappear is still unclear. In addition, premelting is suggested to explain the well-known slipperiness of ice [46–49], but the scope and validity of such explanations are under challenge [50–52].

Notably, these issues are somewhat related to a less-emphasized topic: how the QLL and unpremelted "solid" surface transition into each other. Indeed, the transition kinetics could be important for interpreting results of various studies about premelting, since metastable phases may play a role in them (just like the bulk solid-liquid transition [53]). Additionally, it may also be relevant to more specific phenomena: the appearance of droplets is related to the ice surface converting between multiple structures [30], and the tribology of ice may be affected by the additional melting induced by sliding and pressures [49,54,55]. Therefore, understanding how the QLL appears and freezes would be helpful for both studying premelting and understanding the physics related to premelting. However, few researches have focused on the transition dynamics between the QLL and solid surfaces, and none have provided a microscopic description as far as we know.

Molecular dynamics (MD) simulations have been widely adapted in premelting research [8], because of their molecule-level resolution and ability to finely control external conditions. However, the existing MD studies on premelting are usually not able to capture the transition dynamics, due to their limited spatial and temporal scale. In this paper, we present a picture of the transition dynamics between the QLL and solid surfaces by large-scale MD simulations. In particular, we observed the supercooling and superheating states during the transition, as an analog to their bulk version. Both directions of transition roughly follow the nucleation picture, but also show behavior that is qualitatively different from common scenarios. Notably, the surface inhomogeneity of ice induces the formation of certain nuclei, but they only promote the transition from solid surfaces to the QLL and not inversely. Furthermore, the mismatch of stacking orders between nuclei can hinder the complete freezing of the QLL.

II. METHODS

Conducting an MD simulation starts with choosing a proper force field. Unluckily, this is not an easy task for studying the premelting of ice, especially when the transition process is of interest. As we will show in this work, the premelting transition involves structural features as large as tens of nanometers, and the process can last for hundreds of nanoseconds. Such large spatial and temporal scaling renders fully atomic models such as TIP4P or SPC/E computationally unfeasible. On the other hand, the premelting process involves both bulk and surface molecules and both liquid and solid

*academic_sfc@outlook.com

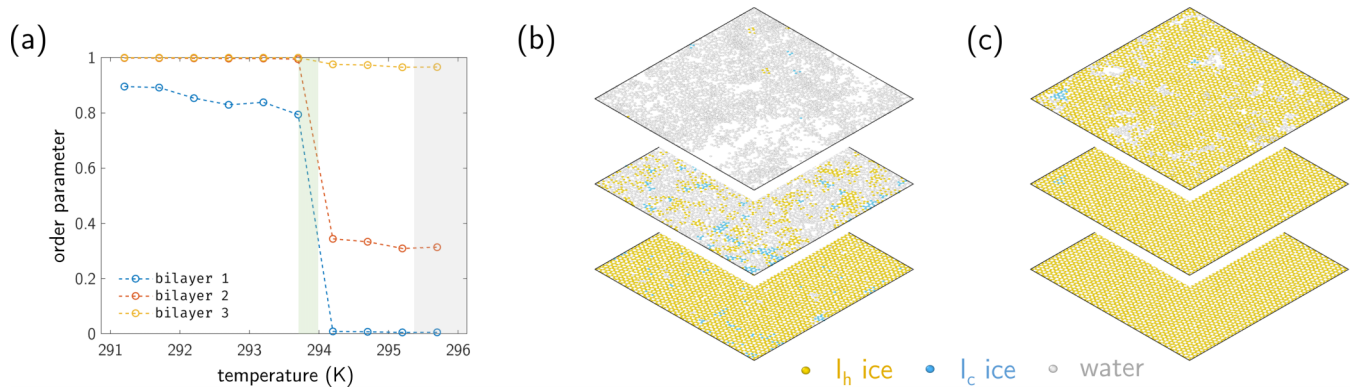

FIG. 1. Overview of the static premelting behavior. (a) The order parameter (proportion of solid molecules) as a function of temperature, for the first three bilayers on the surface. Gray shadow: estimated melting point of ice. Green shadow: estimated onset of premelting (T_p; see Supplemental Material, Sec. 2 [60]). (b) The structure of the QLL at 294.5 K, sliced for the first three bilayers, in a 20 nm × 20 nm simulation cell. Colors represent the structural type of each water molecule (see legends). (c) The structure of the solid surface at 293.1 K.

phases, so the force field needs to be able to describe multiple properties of water and ice. Finally, due to the large discrepancy in experimental results about the premelting of ice [44], their guidance on choosing force fields is limited.

Because of all the reasons above, the optimal choice for this work would be a coarse-grained water model that can reproduce a wide range of physical properties. Coarse-grained water models, by abstracting a water molecule into a single particle, drastically reduce computational cost, thus making large-scale simulations possible. They break the atomic correspondence to the real system, which generally leads to a limited accuracy but can be improved by carefully choosing the function form and parameters. In this work we adopted the ML-mW model [56], a reparametrization of the coarse-grained mW model [57] with improved accuracy on multiple properties. The ML-mW model exhibits a completely premelted first bilayer near the melting point, agreeing with most of the experimental results [44] and also the full atomic TIP4P/ice model (see Appendix A). Its melting point is found to be 295.83 ± 0.5 K by the direct coexistence technique [58,59] (Supplemental Material [60], Sec. 1; also see [61–71]).

To identify how much of the surface is melted, we use the proportion of solid molecules in each bilayer as the order parameter. Namely, each molecule is categorized into one of three types depending on its local structure: (1) hexagonal, (2) cubic, or (3) liquid, by an interleaved version of common neighbor analysis [72]. The order parameter of a bilayer is defined as $1 - N_3/N$, where N is the total number of molecules in the bilayer, and N_3 is that in category (3). Therefore, an order parameter of 1.0 indicates a solid ice crystal and 0.0 means the complete loss of order. Compared to some other choices, this method does not need a somewhat arbitrary number to separate liquid and solid states, and is more robust at solid-liquid interfaces. Appendix B presents a detailed description of how this order parameter works, and compares it with several other options.

The majority of MD simulations are performed with LAMMPS [73] and accelerated by the INTEL [74] or KOKKOS [75] package, with structural visualizations carried out by OVITO [76]. The TIP4P/ice [64] simulations for comparison purposes are performed with GROMACS [77]. The detailed parameters of simulations are available in the Supplemental Material [60]. In this work we primarily focus on the basal (0001) plane, which is commonly exposed on ice surfaces [78]. The Supplemental Material, Sec. 9 [60], briefly discusses the premelting on two prismatic [(10-10) and (11-20)] planes.

III. RESULTS

A. Static premelting profile

Before discussing transition dynamics, it is necessary to determine the static premelting profile: the stable structure of the ice surface at given temperatures. To avoid potential interference from metastable states, this is done by an analog to the direct coexistence technique (see Methods section in the Supplemental Material [60]).

The results for the ML-mW model are summarized in Fig. 1. There is a single specific onset of premelting temperature for the basal plane, where the first two bilayers lose their order simultaneously [Fig. 1(a)]. This onset is further determined as $T_p = 293.85 \pm 0.15$ K (Supplemental Material, Sec. 2 [60]). The premelting behaves like a first-order phase transition, where the order parameters change abruptly at T_p. In the premelted surface with $T > T_p$, the first bilayer is mostly melted and the second bilayer is mixed with solid and liquid [Fig. 1(b)]. In the solid surface with $T < T_p$, only a small fraction of liquid exists in the first bilayer and barely any exists in the second bilayer [Fig. 1(c)]. The proportion of liquid molecules in the first bilayer grows slowly with temperature, but the solid part always dominates when $T < T_p$ [Fig. 1(a)]. The premelting mainly involves the first two bilayers and the third bilayer is mostly intact in both scenarios.

B. Metastable states

The first-order nature of premelting indicates that metastable, or supercooling/superheating states may exist. To verify this, a series of simulations is performed starting from either a solid or a premelted surface, in a range of temperatures near T_p (293.1–294.5 K). Thermodynamically, the melting of solid surfaces should occur under temperatures

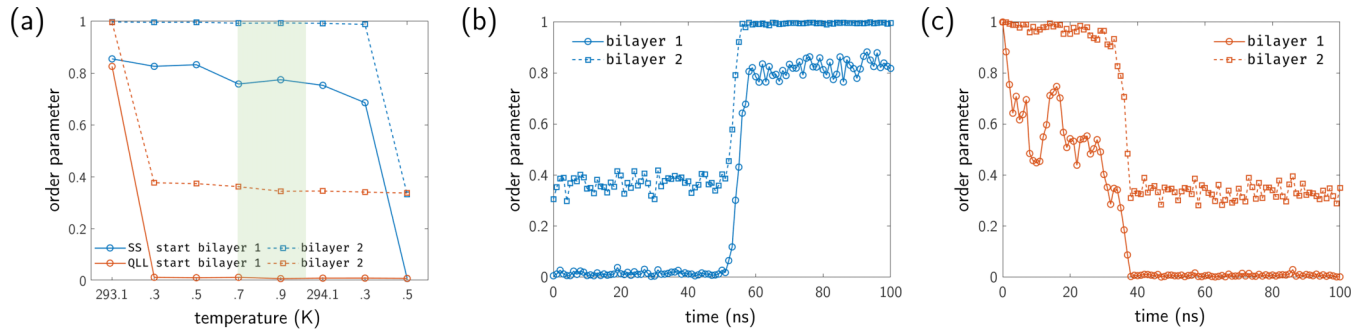

FIG. 2. Supercooling and superheating of the ice surface. (a) The order parameters of first two bilayers, at the end of simulations in 20 nm × 20 nm systems lasting 100 ns each. QLL start = simulations started from QLL (premelted surface); SS = solid surface. Green shadow: estimated onset of premelting. (b) The order parameters of the first two bilayers during a QLL → SS transition at 293.1 K; (c) an SS → QLL transition at 294.5 K.

higher than T_p, and similarly in the opposite direction. Transitions between two phases are indicated by the change of order parameter in first two bilayers.

The results of all such trials are summarized in Fig. 2(a). Notably, the transition between two phases does not occur immediately when it is thermodynamically favored. Indeed, the solid surface is stable in a 100 ns simulation up to 294.3 K, ∼0.5 K higher than T_p, while the melted surface is stable in a 100 ns simulation down to 293.3 K, ∼0.5 K lower than T_p [Fig. 2(a)]. These results indicate the existence of supercooling and superheating for the premelting transition, at least for a short time. These metastable phases bring in a total uncertainty of ∼1 K on the premelting onset, which may be relevant to observations about different measurements of the QLL during heating and cooling [12,18]. This uncertainty is smaller than the discrepancy between the T_p reported by various experiments [44], though. Further uncertainty may come from slow dynamics of the transition at lower temperatures, as suggested in another water model [64] (Supplemental Material, Sec. 3 [60]).

Figures 2(b) and 2(c) demonstrate two instances of transition processes between two phases. Both of them go through some time before an abrupt change of order parameters, confirming the existence of metastable phases. However, the premelting and freezing transitions also show different features: the first bilayer of the supercooled phase has a stable order parameter before transition [Fig. 2(b)], but that of the superheated phase fluctuates rather heavily [Fig. 2(c)]. This is similar to the impression of its bulk counterpart, where supercooling is considered much more stable than superheating [79]. Such contrast also implies a difference in the transition mechanism between two directions, as we will discuss soon.

C. Transition dynamics: Premelting

To further investigate the transition mechanism between two phases, we performed large-scale (70 nm × 70 nm) MD simulations and visualized the structural change of ice surfaces. The conditions are selected so that (1) the metastable phases can exist for a reasonably long time so they are meaningful; (2) transitions are still observable in the timescale of an MD simulation. Five independent runs are performed in each direction, with different random seeds for initial velocities.

Figure 3 shows a typical trajectory of the premelting direction: from solid surface to QLL. In the beginning, the first bilayer is a regular mixture of solid and liquid (a1), similar to the equilibrium state at lower temperatures [Fig. 1(c)]. After some time, however, holes start to appear in the first bilayer [(a2), circled]; meanwhile, some liquid regions in the second bilayer become larger [(b2), circled]. One liquid region in the second bilayer grows further later [(b3), circled], with larger holes and liquid region in the corresponding first bilayer [(a3), circled]. The liquid region continues to grow (a4,b4) until it occupies the whole surface, completing the phase transition. All five independent runs show a similar procedure of premelting, only with some difference in the transition time (100–250 ns).

The role of holes in premelting deserves attention. Generally speaking, holes are intrinsic features of the ice surface near the melting point: they exist both below and above the premelting onset (Fig. 4). Furthermore, they play a special role in premelting: note that the growing liquid region in Fig. 3(b) is located close to a large hole in Fig. 3(a), and it is not a coincidence. Namely, liquid molecules in the second bilayer are more likely to appear near or under holes in the first bilayer (Supplemental Material, Sec. 4 [60]). In other words, holes lead to a surface inhomogeneity favoring the premelting transition, which requires the second bilayer to lose most of its order. This effect arguably comes from two aspects: (1) holes in the first bilayer directly expose those regions of the second bilayer to the air, making them more vulnerable to thermal perturbations; (2) liquid regions are sometimes found near holes in the first bilayer [see Figs. 3(a2) and 4(a), for example], so the region beneath them more likely consists of liquid too.

It is helpful to compare premelting with its more familiar counterpart, the bulk liquid-solid transition. In the latter scenario, the supercooling/superheating phases turn into stable phases by a nucleation process: nuclei (i.e., small regions) of the stable phase are randomly generated by thermal fluctuations, and nuclei large enough can grow continuously into bulk [80]. In the premelting transition, the liquid regions in the second bilayer [Fig. 3(b)]

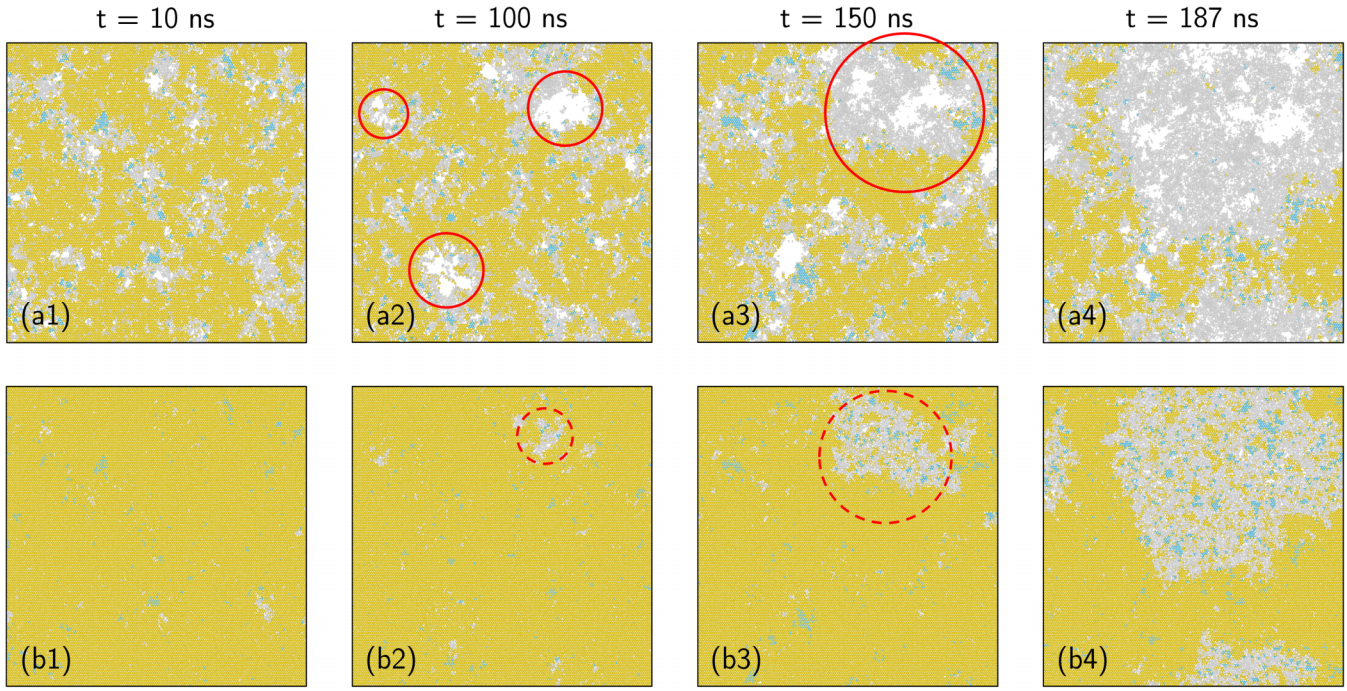

FIG. 3. The structure of the ice surface during a solid → premelted transition. Colors represent different structural types (see legends in Fig. 1). Pure white means no molecules in that region of the bilayer, i.e., holes. The system size is ∼70 nm × 70 nm. The simulation is performed at 294.2 K, starting from a perfect ice surface. (a1)–(a4) The first bilayer, at 10, 100, 150, and 187 ns of the simulation. (b1)–(b4) The second bilayer. Some holes and liquid nuclei are circled (see main text).

may be similarly considered as nuclei. The difference, however, is manifested by considering two bilayers together: nuclei are much more likely to form near or under holes in the first bilayer, instead of being uniformly distributed.

D. Transition dynamics: Freezing

A typical trajectory of the freezing direction, where the QLL turns into the solid surface, is illustrated in Fig. 5. Similarly, holes are found in the first bilayer of the QLL [Fig. 5(a), circled in (a1,a2); also see Fig. 4(b)]. In the beginning, the second bilayer is mainly composed of liquid, with solid islands of varied sizes straggling in it (b1). After some time, large solid islands appear in the second bilayer where holes in the first bilayer locate [(b2,a2), circled]. At first glance, this seems to be an analog to the premelting direction discussed earlier (Fig. 3): holes in the first bilayer help the formation of solid nuclei (i.e., the large solid islands) and promote the phase transition. However, the large nuclei under the holes do not grow further in this case. Indeed, it is another nucleus away from the holes that finally grows larger [(a3,b3), circled], and spreads into the whole surface (a4,b4). This is not a coincidence either: though large nuclei can form under holes, they are unlikely to induce freezing (Supplemental Material, Sec. 5 [60]). This is different from its bulk counterpart, where the nuclei size is the key factor in triggering phase transitions. Indeed, nuclei under holes only induce freezing in one of the five independent runs, and it takes a rather long time (Fig. S7 in the Supplemental Material [60]).

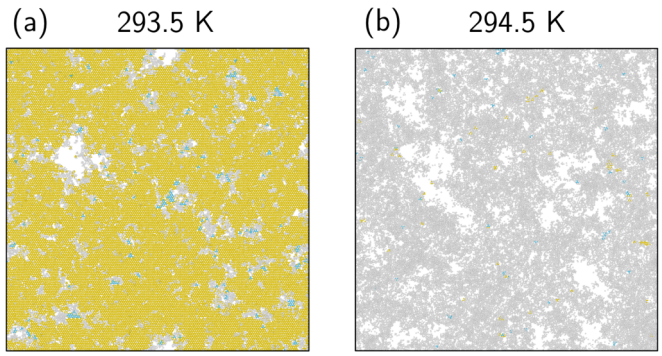

FIG. 4. Structures of the first bilayer, in ∼70 nm × 70 nm simulation cells: (a) the solid surface at 293.5 K; (b) the QLL at 294.5 K. Note that both structures are in their stable phases and contain holes (empty spaces).

Such observation reveals the different roles of holes during surface melting and freezing: though holes exist in both scenarios, they seem to only promote the transition to premelted phases, but not reversely. From another perspective, though large nuclei under holes exist in both scenarios, they only significantly contribute to premelting but not freezing. This contrast probably traces back to the origin of holes on ice surfaces: the molecule redistribution between bilayers. Namely, molecules in the first bilayer move into lower and upper layers during premelting (Supplemental Material, Sec. 6 [60]), resulting in lower molecule density, thus growing holes (Supplemental Material, Sec. 7 [60]). Growing holes allows the nuclei under the holes to grow, which may further trigger

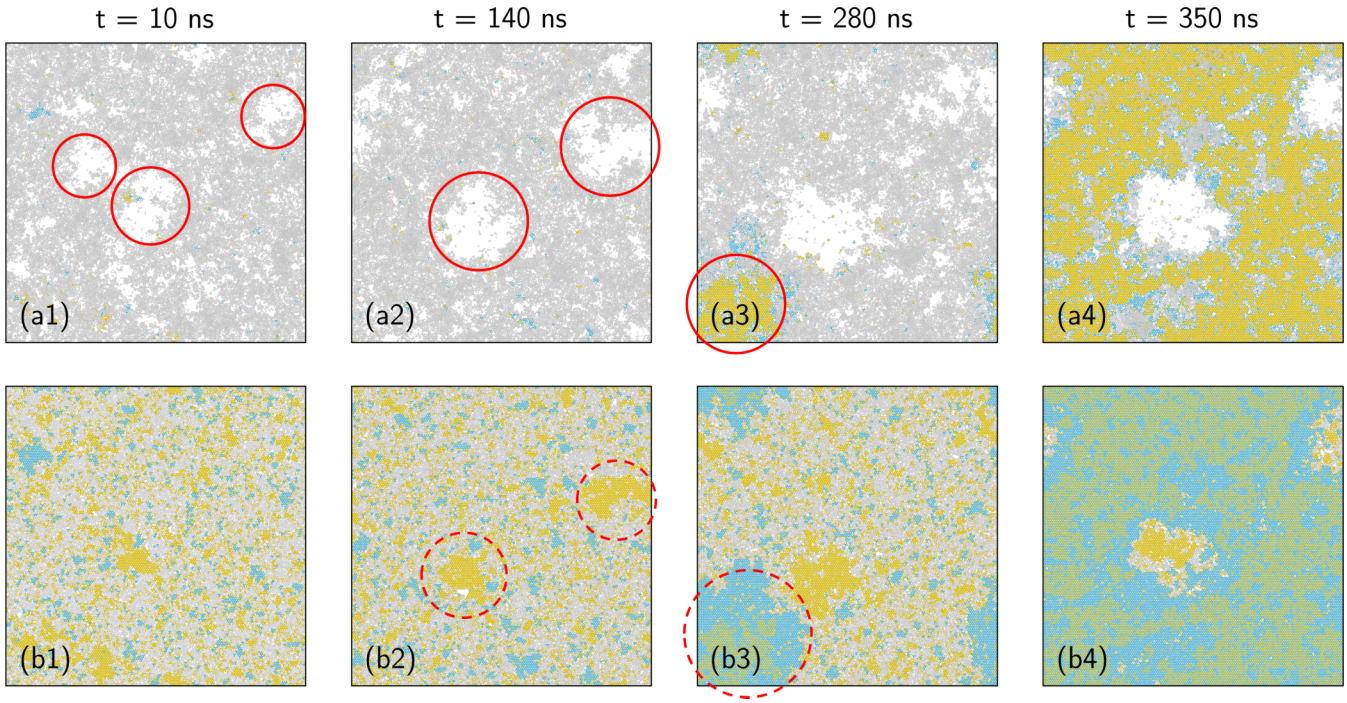

FIG. 5. The structure of the ice surface during a premelted → solid transition. Colors represent different structural types (see legends in Fig. 1). The system size is ∼70 nm × 70 nm. The simulation is performed at 293.3 K, starting from a premelted surface. (a1)–(a4) The first bilayer, at 10, 140, 280, and 350 ns of the simulation. (b1)–(b4) The second bilayer. Some holes and solid nuclei are circled (see main text).

the phase transition. In the freezing process, however, holes tend to shrink instead (Supplemental Material, Sec. 7 [60]), confining the nuclei under them and preventing them from spreading into the whole surface. Therefore, holes do not help the transition to the freezing phase.

Another notable thing is that the solid grown from the supercooled QLL is partially stacking disordered ice [(b3,b4), cubic molecules shown as blue]. This is observed in two out of five runs, indicating that such stacking disorders might also exist in real ice surfaces frozen from the QLL. This hypothesis is further supported by the belief that stacking disordered ice is kinetically favored during crystallization [81]. Furthermore, molecules from different nuclei (e.g., under holes) may have different stacking orders within the second bilayer (b3), because of their different origin. As a result, the boundary region between stacking orders remains liquid to the end of simulation (b4) due to lattice mismatch. The lifetime of such boundaries is unknown yet, but they might survive longer if the holes in the first bilayer are large, which could result from holes merging to reduce their "edge" energy in a longer timescale.

IV. DISCUSSION

So far, we have shown the surface inhomogeneity of QLL and its implication for the transition dynamics. In real scenarios, the ice surface may undergo growth or evaporation. Such processes can lead to an ice surface not being terminated with one full bilayer, altering the surface structure including the inhomogeneity. Specifically, excess molecules beyond one bilayer can "fill" the holes and ultimately lead to raised clusters on the surface (Supplemental Material, Sec. 8 [60]). On a sufficiently large spatial and temporal scale, these holes or clusters may grow larger and go beyond a single bilayer, resulting in macroscopic inhomogeneity on ice surfaces. Similar inhomogeneity is already observed in experiments with optical microscopy [30], and is suggested in a continuous model [28]. It is desirable that such macroscopic feature (usually at ∼10 μm or larger) can be directly generated from the molecular level.

In this study we used the ML-mW water model, which shows a first-order premelting transition at several kelvins below the melting point (Fig. 1). Though this model can describe many properties of water with good accuracy [56], it cannot be perfect due to the empirical and coarse-grained nature. For example, the diffusion coefficient of water reported by the ML-mW model is ∼2× the experimental value [56]. Therefore, the conclusion of this work should not be considered as definitive. Indeed, models like the original mW show a completely continuous premelting transition [21,45], and the premelting onset reported by different simulations can differ by dozens of kelvins [11,15,21,25,26,45]. Therefore it is not surprising if other water models have different premelting dynamics, not to mention experiments with highly variable conditions. However, currently it is difficult to remove this ambiguity, as we have to rely on empirical classical force fields for computational efficiency. These force fields are usually built with the main focus on bulk properties [56,57,64], making them less reliable for premelting studies. To move towards a more definitive conclusion, an efficient force field of water that can accurately represent the ice surface is desired. Nevertheless, we still feel it helpful to provide a potential picture of the transition dynamics here, indicating the importance of metastable phases, and showing

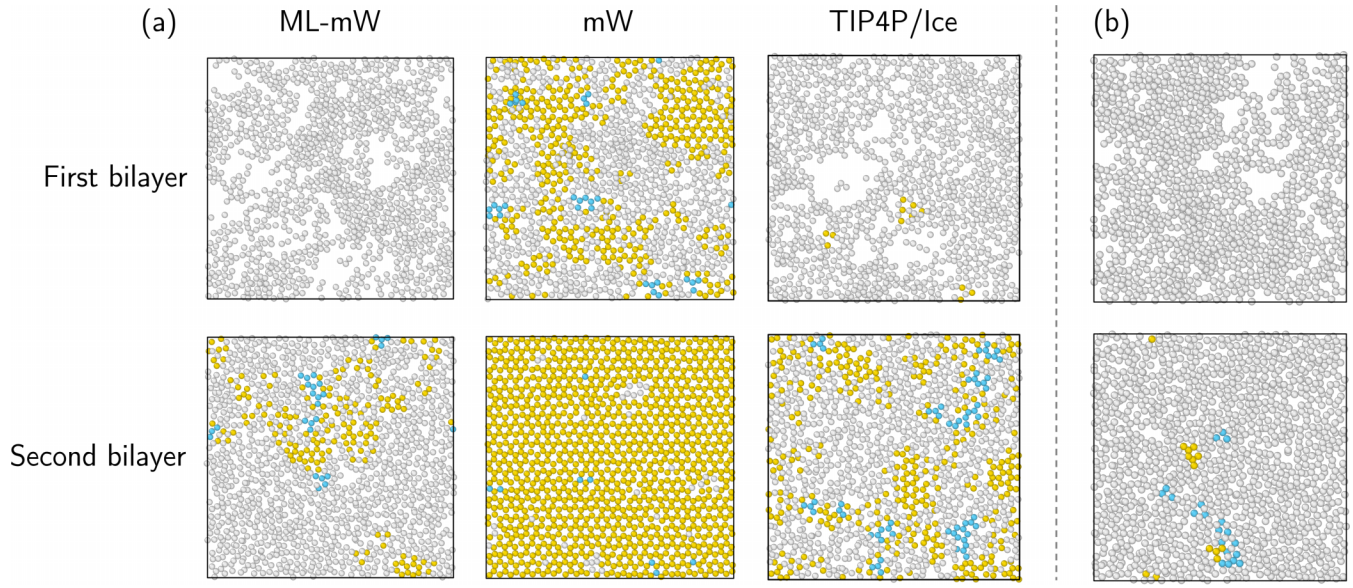

FIG. 6. Ice surface near melting point in three water models, sliced for the first and second bilayers. Colors represent structural types (see Fig. 1). Only oxygen atoms are shown for TIP4P/ice. (a) Ice surfaces after 10 ns of simulation each. Temperature: ML-mW → 295.7 K($T_m - 0.13$ K), mW → 275.7 K ($T_m + 1$ K [57]), TIP4P/ice → 270 K ($T_m + 0.2$ K [58]). (b) The ice surface of the mW model after rapidly throwing molecules and 25 ns of simulation (throw at the rate of 0.2 molecules/fs, with initial velocities of 0.2–0.3 nm/ps towards the surface. One bilayer is thrown in total). The ice surfaces keep a similar structure in the 25 ns simulation; i.e., it is at least a metastable phase.

how the QLL may behave under a scaling not frequently reached.

V. CONCLUSION

In this work, we have provided a molecular-level picture of the transition dynamics between the premelted and solid ice surfaces. Supercooling and superheating phases exist in the premelting transition, and generally the supercooled phase has smaller fluctuation. The transition between phases roughly follows the nucleation picture, and holes in ice surfaces promote nuclei generation. Nuclei induced by holes can grow and lead to a full transition to the premelting phase, but not to the inverse direction. Sometimes the freezing process leads to the coexistence of different stacking orders in the same bilayer, due to having multiple nuclei concurrently. Further studies may focus on developing water models that specifically target ice surfaces, and reevaluating the premelting behavior of ice including transition dynamics [85].

ACKNOWLEDGMENTS

This work was supported by the National Natural Science Foundation of China under Grant No. 11974024; we thank Prof. Ji Chen for providing computational resources.

APPENDIX A: EXISTENCE OF COMPLETE PREMELTING IN SEVERAL WATER MODELS

In this section, we will compare the stable surface structures of three water models (mW, ML-mW, TIP4P/ice) near the melting point. To this end, a 10 nm × 10 nm perfect ice surface is built for each of these three models, and they are simulated near the melting point of each model for 10 ns. The results are shown in Fig. 6.

The ML-mW and TIP4P/ice models share similar features near the melting point: the first bilayer is almost completely melted, while the second bilayer is mainly liquid with some solid islands in them [Fig. 6(a)]. However, the original mW model is very different: the first bilayer is only partially melted at a temperature higher than the melting point, and the second bilayer is still mostly solid [Fig. 6(a)]. In other words, the mW ice never completely premelts. To eliminate the effect of potential metastable phases, we tried to artificially make a completely premelted surface for the mW model by rapidly throwing molecules to the surface. It turns out that the mW model could have a completely premelted phase [Fig. 6(b), also see captions], but coexistence tests reveal that it is only metastable even above the melting point (not shown here). Therefore, the mW model does not seem to have a thermodynamically stable complete premelting, while two other models have.

Such difference points out the importance of force field choice in premelting studies. Note, however, that it does not mean ML-mW and TIP4P/ice are completely the same in premelting behavior. Indeed, the TIP4P/ice model is reported to show premelting down to 200 K [10] (also see Supplemental Material, Sec. 3 [60]), while the ML-mW shows that only at several kelvins below the melting point. Nevertheless, the comparison indicates that the ML-mW model is a reasonable choice for premelting studies, especially when the large scaling of simulations prohibits using fully atomic models.

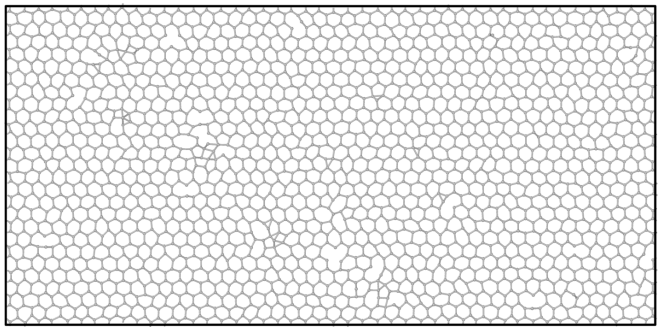

FIG. 7. A typical structure of the third bilayer at 295.2 K, with the first two bilayers premelted. The system size is ∼20 nm × 10 nm. Bonds are drawn for visualization only; they are not used in analysis.

APPENDIX B: ORDER PARAMETER

The molecules in ice surfaces are categorized by their local structures through this work, by the method described in Appendix A of Ref. [72]. This method is originally purposed for the Ge/Si system but is also applicable for systems with similar lattices, such as ice [35]. It exploits the fact that the I_h ice consists of two interleaved hcp lattices, and the I_c ice consists of two interleaved fcc lattices; therefore, we can determine the structure type of a molecule by checking out if that molecule and its *second* neighbors form an fcc/hcp lattice. The latter task can be done by the widely used common neighbor analysis (CNA) [82], which works by classifying neighbor molecule pairs by their local environments; readers are redirected to Ref. [82] for details of CNA. The procedure of the whole analysis is summarized below:

(1) Select a molecule ("central molecule") to be identified.

(2) Find four nearest neighbors of the central molecule ("first neighbors").

(3) Find four nearest neighbors for each of the first neighbors ("second neighbors"). This should give 12 molecules in total, excluding the central molecule itself (which is counted four times).

(4) Perform CNA on the central molecule and second neighbors. The cutoff radius of CNA is $r_{\mathrm{CNA}} = r_0(1 + \sqrt{2})/2$, where r_0 is the average distance of twelve second neighbors from the central molecule. For the central molecule of I_c ice, all center-neighbor molecule pairs are of the 421 type, while for I_h ice, half of them are 421 and half are 422 [82].

By repeatedly performing the procedure above, all water molecules can be categorized into the following groups:

(a) A central molecule of I_h ice.

(b) A central molecule of I_c ice.

(c) Does not belong to (a) or (b), but is a first neighbor of a group (a) molecule.

(d) Does not belong to (a) or (b), but is a first neighbor of a group (b) molecule.

(e) Does not belong to (a)–(d), but is a second neighbor of a group (a) molecule.

(f) Does not belong to (a)–(d), but is a second neighbor of a group (b) molecule.

(g) None of the above.

For our purpose, the structure type "hexagonal (I_h)" corresponds to groups (a), (c), and (e); the "cubic (I_c)" corresponds to (b), (d), and (f); and the "liquid" corresponds to (g). Note that it is correct to consider groups (c)–(f) as solid molecules: these molecules themselves are "on site" though some of their neighbors are not. This ensures the surface molecules are correctly categorized (i.e., a perfect ice surface has an order parameter of 1). For the three-atom TIP4P/ice model, only oxygen atoms are considered during the identification.

It is possible for a molecule to be eligible for both (c) and (d), or both (e) and (f). Usually this occurs at the boundary of I_h and I_c ice, where the local structure may be equivalently interpreted as either. Anyway, the order parameter itself is always well defined.

Note that this approach is mostly based on geometrical arguments, so there is no need for an arbitrary number to separate two phases. In addition, it is also more robust at solid-liquid interfaces compared to some other choices. Such scenarios occur in the bilayer right under the QLL, e.g., the third bilayer in the premelted surface. Figure 7 shows a typical structure of the third bilayer at 295.2 K, with the first two bilayers premelted. The bilayer largely keeps the hexagonal structure with only occasional defects, indicating that the order parameter should be close to its maximum. Table I shows the order parameter reported by three different definitions. The one used in this work reports ∼2.1% of melting, which is reasonable considering the existence of defects. However, the two other choices report much higher percentages.

Figure 8 recalculates the static premelting profile [Fig. 1(a)] under several order parameters. The exact behavior differs, but all of them suggest a first-order type transition at the same temperature and a QLL of ∼two bilayers, agreeing with Fig. 1(a).

TABLE I. The order parameter under three definitions, and the corresponding percentile in their possible ranges. The lower limit is estimated by the first bilayer of the premelted surface, and the upper limit is estimated by the innermost movable (eighth) bilayer of the system. The percentile may be interpreted as how much of the bilayer has melted (0% = as melted as the first bilayer, 100% = as solid as the innermost bilayer). See captions of Fig. 8 for definitions of the last two order parameters.

	This work [72]	Local tetrahedrality [83]	Local Steinhardt $\boldsymbol{q}_6$ [84]
Value	0.9787	0.8872	0.5390
Possible range	[∼0.005, 1]	[∼0.65, ∼0.97]	[∼0.25, ∼0.74]
Percentile (% melted)	∼2.1	∼26	∼41

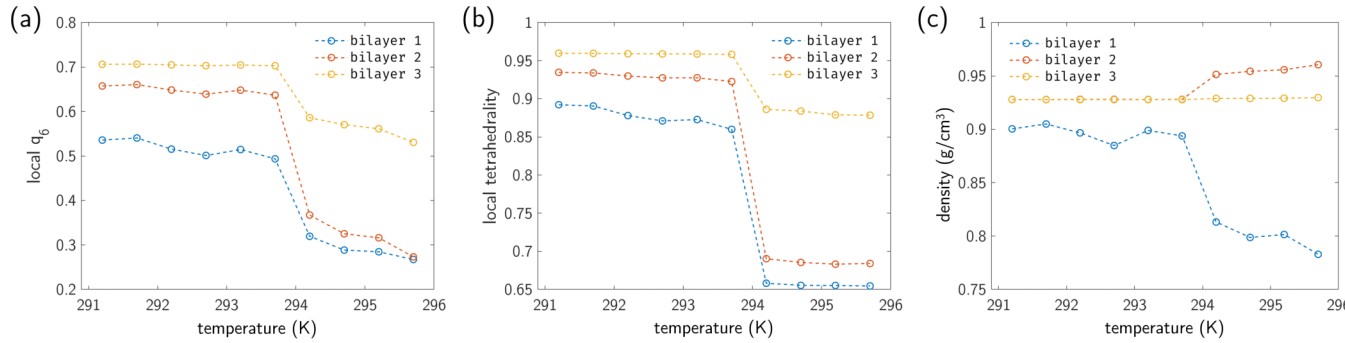

FIG. 8. The static premelting profile in Fig. 1(a) under several order parameters. (a) The local Steinhardt parameter q_6, defined for each molecule i as $\frac{1}{n}\sum_j[\boldsymbol{q}_6(i)\cdot\boldsymbol{q}_6(j)]$, where $\boldsymbol{q}_6$ is a 13-vector $(q_{6(-6)}, q_{6(-5)}, \ldots, q_{6(6)})$ defined as $q_{6m}(i)=\frac{1}{n}\sum_j Y_{6m}(\boldsymbol{r}_{ij})$. In these expressions, n is the number of molecules in the first coordination sphere (<0.34 nm) of i, the summation over j includes all molecules in that sphere, $\boldsymbol{r}_{ij}$ is the distance vector between i and j, and Y_{6m} are sixth-order spherical harmonics. This parameter is calculated using PLUMED [84]. (b) The local tetrahedrality [83], defined for each molecule i as $(1-\frac{9}{2n(n-1)}\sum_{\langle j,k\rangle}(\cos\theta_{jik}+\frac{1}{3})^2)$, where θ_{jik} is the angle formed by molecules j, i, k, and the summation over j, k includes all pairs of molecules in the first coordination sphere of i. Note that the "un-normalized" tetrahedrality [85], where the coordination number n is always 4, is not a good choice for premelting studies since molecules are undercoordinated on surfaces. (c) The density, defined for each bilayer as $\frac{NM}{Ah}$, where N is the number of molecules in the bilayer, M is the mass of a water molecule, A is the surface area of the system, and h is the height of a single bilayer (0.734 87/2 nm). The opposite trend of density change in the first two bilayers reflects the molecule redistribution during premelting (Supplemental Material, Sec. 6 [60]).

[1] M. R. Faraday, On certain conditions of freezing water, Athenaeum **1181**, 640 (1850).

[2] J. G. Dash, H. Fu, and J. S. Wettlaufer, The premelting of ice and its environmental consequences, Rep. Prog. Phys. **58**, 115 (1995).

[3] J. S. Wettlaufer and J. Vachier, Premelting controlled active matter in ice, Phys. Rev. E **105**, 024601 (2022).

[4] E. J. N. Kuiper, J. H. P. de Bresser, M. R. Drury, J. Eichler, G. M. Pennock, and I. Weikusat, Using a composite flow law to model deformation in the NEEM deep ice core, Greenland—Part 2: The role of grain size and premelting on ice deformation at high homologous temperature, Cryosphere **14**, 2449 (2020).

[5] F. Yu, P. Guo, Y. Lai, and D. Stolle, Frost heave and thaw consolidation modelling. Part 1: A water flux function for frost heaving, Can. Geotech. J. **57**, 1581 (2019).

[6] Y. Li and G. A. Somorjai, Surface premelting of ice, J. Phys. Chem. C **111**, 9631 (2007).

[7] Y. Nagata, T. Hama, E. H. G. Backus, M. Mezger, D. Bonn, M. Bonn, and G. Sazaki, The surface of ice under equilibrium and nonequilibrium conditions, Acc. Chem. Res. **52**, 1006 (2019).

[8] B. Slater and A. Michaelides, Surface premelting of water ice, Nat. Rev. Chem. **3**, 172 (2019).

[9] N. Orndorf, S. Singla, and A. Dhinojwala, Transition in the acid–base component of surface free energy of ice upon the premelting of its second molecular bilayer, J. Phys. Chem. C **124**, 19588 (2020).

[10] T. Sugimoto, Y. Otsuki, T. Ishiyama, A. Morita, K. Watanabe, and Y. Matsumoto, Topologically disordered mesophase at the topmost surface layer of crystalline ice between 120 and 200 K, Phys. Rev. B **99**, 121402(R) (2019).

[11] M. A. Sánchez, T. Kling, T. Ishiyama, M. van Zadel, P. J. Bisson, M. Mezger, M. N. Jochum, J. D. Cyran, W. J. Smit, H. J. Bakker, M. J. Shultz, A. Morita, D. Donadio, Y. Nagata, M. Bonn, and E. H. G. Backus, Experimental and theoretical evidence for bilayer-by-bilayer surface melting of crystalline ice, Proc. Natl. Acad. Sci. USA **114**, 227 (2017).

[12] H. Dosch, A. Lied, and J. H. Bilgram, Glancing-angle x-ray scattering studies of the premelting of ice surfaces, Surf. Sci. **327**, 145 (1995).

[13] A. Kouchi, Y. Furukawa, and T. Kuroda, X-ray diffraction pattern of quasi-liquid layer on ice crystal surface, J. Phys. Colloq. **48**, 675 (1987).

[14] D. Nason and N. H. Fletcher, Photoemission from ice and water surfaces: Quasiliquid layer effect, J. Chem. Phys. **62**, 4444 (1975).

[15] G. Kroes, Surface melting of the (0001) face of TIP4P ice, Surf. Sci. **275**, 365 (1992).

[16] J. Gelman Constantin, M. M. Gianetti, M. P. Longinotti, and H. R. Corti, The quasi-liquid layer of ice revisited: The role of temperature gradients and tip chemistry in AFM studies, Atmos. Chem. Phys. **18**, 14965 (2018).

[17] H. Li, M. Bier, J. Mars, H. Weiss, A. Dippel, O. Gutowski, V. Honkimäki, and M. Mezger, Interfacial premelting of ice in nano composite materials, Phys. Chem. Chem. Phys. **21**, 3734 (2019).

[18] M. Elbaum, S. G. Lipson, and J. G. Dash, Optical study of surface melting on ice, J. Cryst. Growth **129**, 491 (1993).

[19] M. M. Conde, C. Vega, and A. Patrykiejew, The thickness of a liquid layer on the free surface of ice as obtained from computer simulation, J. Chem. Phys. **129**, 14702 (2008).

[20] M. A. Carignano, P. B. Shepson, and I. Szleifer, Molecular dynamics simulations of ice growth from supercooled water, Mol. Phys. **103**, 2957 (2005).

[21] I. Pickering, M. Paleico, Y. A. P. Sirkin, D. A. Scherlis, and M. H. Factorovich, Grand canonical investigation of the quasi liquid layer of ice: Is it liquid?, J. Phys. Chem. B **122**, 4880 (2018).

[22] P. Llombart, E. G. Noya, D. N. Sibley, A. J. Archer, and L. G. MacDowell, Rounded Layering Transitions on the Surface of Ice, Phys. Rev. Lett. **124**, 065702 (2020).

[23] H. Niinomi, T. Yamazaki, H. Nada, T. Hama, A. Kouchi, J. T. Okada, J. Nozawa, S. Uda, and Y. Kimura, High-density liquid water at a water–ice interface, J. Phys. Chem. Lett. **11**, 6779 (2020).

[24] T. Kling, F. Kling, and D. Donadio, Structure and dynamics of the quasi-liquid layer at the surface of ice from molecular simulations, J. Phys. Chem. C **122**, 24780 (2018).

[25] J. Benet, P. Llombart, E. Sanz, and L. G. MacDowell, Premelting-Induced Smoothening of the Ice-Vapor Interface, Phys. Rev. Lett. **117**, 096101 (2016).

[26] C. L. Bishop, D. Pan, L. M. Liu, G. A. Tribello, A. Michaelides, E. G. Wang, and B. Slater, On thin ice: Surface order and disorder during pre-melting, Faraday Discuss. **141**, 277 (2009).

[27] P. Llombart, E. G. Noya, and L. G. MacDowell, Surface phase transitions and crystal habits of ice in the atmosphere, Sci. Adv. **6**, 9322 (2020).

[28] D. N. Sibley, P. Llombart, E. G. Noya, A. J. Archer, and L. G. MacDowell, How ice grows from premelting films and water droplets, Nat. Commun. **12**, 239 (2021).

[29] K. Nagashima, G. Sazaki, and K. Murata, *In situ* observations of spiral growth on ice crystal surfaces, Phys. Rev. Mater. **2**, 093402 (2018).

[30] K. I. Murata, H. Asakawa, K. Nagashima, Y. Furukawa, and G. Sazaki, Thermodynamic origin of surface melting on ice crystals, Proc. Natl. Acad. Sci. USA **113**, E6741 (2016).

[31] K. I. Murata, K. Nagashima, and G. Sazaki, How Do Ice Crystals Grow inside Quasiliquid Layers? Phys. Rev. Lett. **122**, 026102 (2019).

[32] A. Hudait and V. Molinero, What determines the ice polymorph in clouds? J. Am. Chem. Soc. **138**, 8958 (2016).

[33] Y. Ahn, J. Kim, and K. Kim, Activation of peroxymonosulfate by bicarbonate and acceleration of the reaction by freezing, Sci. Total Environ. **785**, 147369 (2021).

[34] S. P. Niblett and D. T. Limmer, Ion dissociation dynamics in an aqueous premelting layer, J. Phys. Chem. B **125**, 2174 (2021).

[35] I. de Almeida Ribeiro, R. Gomes De Aguiar Veiga, and M. de Koning, Effect of sodium chloride on internal quasi-liquid layers in ice I_h, J. Phys. Chem. C **125**, 18526 (2021).

[36] P. P. A. Malley, S. Chakraborty, and T. F. Kahan, Physical characterization of frozen saltwater solutions using Raman microscopy, ACS Earth Space Chem **2**, 702 (2018).

[37] A. S. McFall, K. C. Edwards, and C. Anastasio, Nitrate photochemistry at the air–ice interface and in other ice reservoirs, Environ. Sci. Technol. **52**, 5710 (2018).

[38] T. Bartels-Rausch, F. Orlando, X. Kong, L. Artiglia, and M. Ammann, Experimental evidence for the formation of solvation shells by soluble species at a nonuniform air–ice interface, ACS Earth Space Chem **1**, 572 (2017).

[39] H. Li, J. Mars, W. Lohstroh, M. M. Koza, H. J. Butt, and M. Mezger, Water mobility in the interfacial liquid layer of ice/clay nanocomposites, Angew. Chem., Int. Ed. **60**, 7697 (2021).

[40] T. Verhagen, J. Klimes, B. Pacakova, M. Kalbac, and J. Vejpravova, Anomalous freezing of low-dimensional water confined in graphene nanowrinkles, ACS Nano **14**, 15587 (2020).

[41] Y. Wang, Y. Guo, and W. Guo, Screening effect of monolayer van der Waals crystals on surface deicing: A molecular simulation study, Phys. Chem. Chem. Phys. **22**, 27873 (2020).

[42] H. Reichert, H. Dosch, J. Bilgram, V. Honkimäki, A. Snigirev, and S. Engemann, Interfacial Melting of Ice in Contact with SiO_2, Phys. Rev. Lett. **92**, 205701 (2004).

[43] D. Chen, M. D. Gelenter, M. Hong, R. E. Cohen, and G. H. McKinley, Icephobic surfaces induced by interfacial nonfrozen water, ACS Appl. Mater. Interfaces **9**, 4202 (2017).

[44] K. Kim and M. J. Park, Ice-assisted synthesis of functional nanomaterials: The use of quasi-liquid layers as nanoreactors and reaction accelerators, Nanoscale **12**, 14320 (2020).

[45] Y. Qiu and V. Molinero, Why is it so difficult to identify the onset of ice premelting? J. Phys. Chem. Lett. **9**, 5179 (2018).

[46] L. Canale, J. Comtet, A. Nigues, C. Cohen, C. Clanet, A. Siria, and L. Bocquet, Nanorheology of Interfacial Water During Ice Gliding, Phys. Rev. X **9**, 041025 (2019).

[47] P. B. Louden and J. D. Gezelter, Why is ice slippery? Simulations of shear viscosity of the quasi-liquid layer on ice, J. Phys. Chem. Lett. **9**, 3686 (2018).

[48] B. N. J. Persson, Ice friction: Role of non-uniform frictional heating and ice premelting, J. Chem. Phys. **143**, 224701 (2015).

[49] B. Weber, Y. Nagata, S. Ketzetzi, F. Tang, W. J. Smit, H. J. Bakker, E. H. G. Backus, M. Bonn, and D. Bonn, Molecular insight into the slipperiness of ice, J. Phys. Chem. Lett. **9**, 2838 (2018).

[50] J. H. Lever, E. Asenath-Smith, S. Taylor, and A. P. Lines, Assessing the mechanisms thought to govern ice and snow friction and their interplay with substrate brittle behavior, Front. Mech. Eng. **7**, 690425 (2021).

[51] J. H. Lever, A. P. Lines, S. Taylor, G. R. Hoch, E. Asenath-Smith, and D. S. Sodhi, Revisiting mechanics of ice–skate friction: From experiments at a skating rink to a unified hypothesis, J. Glaciol. **68**, 337 (2021).

[52] L. Makkonen and M. Tikanmäki, Modeling the friction of ice, Cold Reg. Sci. Technol. **102**, 84 (2014).

[53] P. Gallo, K. Amann-Winkel, C. A. Angell, M. A. Anisimov, F. Caupin, C. Chakravarty, E. Lascaris, T. Loerting, A. Z. Panagiotopoulos, J. Russo, J. A. Sellberg, H. E. Stanley, H. Tanaka, C. Vega, L. Xu, and L. G. M. Pettersson, Water: A tale of two liquids, Chem. Rev. **116**, 7463 (2016).

[54] P. A. Santos-Flórez, C. J. Ruestes, and M. de Koning, Atomistic simulation of nanoindentation of ice I_h, J. Phys. Chem. C **124**, 9329 (2020).

[55] A. Kriston, N. A. Isitman, T. Fülöp, and A. J. Tuononen, Structural evolution and wear of ice surface during rubber–ice contact, Tribol. Int. **93**, 257 (2016).

[56] H. Chan, M. J. Cherukara, B. Narayanan, T. D. Loeffler, C. Benmore, S. K. Gray, and S. K. R. S. Sankaranarayanan, Machine learning coarse grained models for water, Nat. Commun. **10**, 379 (2019).

[57] V. Molinero and E. B. Moore, Water modeled as an intermediate element between carbon and silicon, J. Phys. Chem. B **113**, 4008 (2009).

[58] M. M. Conde, M. Rovere, and P. Gallo, High precision determination of the melting points of water TIP4P/2005 and water TIP4P/ice models by the direct coexistence technique, J. Chem. Phys. **147**, 244506 (2017).

[59] A. J. C. Ladd and L. V. Woodcock, Triple-point coexistence properties of the Lennard-Jones system, Chem. Phys. Lett. **51**, 155 (1977).

[60] See Supplemental Material at http://link.aps.org/supplemental/10.1103/PhysRevB.108.045413 for details of simulation

methods, the melting point and premelting onset of the ML-mW model, slow transition dynamics of ice surfaces under low temperatures, effect of holes on the distribution of liquid molecules, indication that solid nuclei under holes are unlikely to induce freezing, redistribution of molecules between bilayers during premelting, the trend of hole sizes during premelting and freezing, QLL with excess molecules on the surface, the static premelting profile of (10-10) and (11-20) planes; this also contains Refs. [19,61–71].

[61] W. G. Hoover, Canonical dynamics: Equilibrium phase-space distributions, Phys. Rev. A **31**, 1695 (1985).

[62] S. Nosé, A unified formulation of the constant temperature molecular dynamics methods, J. Chem. Phys. **81**, 511 (1984).

[63] S. Cui, H. Chen, and Z. Zhao, Premelting layer during ice growth: Role of clusters, Phys. Chem. Chem. Phys. **24**, 15330 (2022).

[64] J. L. F. Abascal, E. Sanz, F. R. García, and C. Vega, A potential model for the study of ices and amorphous water: TIP4P/ice, J. Chem. Phys. **122**, 234511 (2005).

[65] M. Matsumoto, T. Yagasaki, and H. Tanaka, Novel algorithm to generate hydrogen-disordered ice structures, J. Chem. Inf. Model. **61**, 2542 (2021).

[66] M. Matsumoto, T. Yagasaki, and H. Tanaka, GenIce: Hydrogen-disordered ice generator, J. Comput. Chem. **39**, 61 (2017).

[67] D. Frenkel, Simulations: The dark side, Eur. Phys. J. Plus **128**, 10 (2013).

[68] J. R. Espinosa, E. Sanz, C. Valeriani, and C. Vega, On fluid-solid direct coexistence simulations: The pseudo-hard sphere model, J. Chem. Phys. **139**, 144502 (2013).

[69] H. Edelsbrunner, D. Kirkpatrick, and R. Seidel, On the shape of a set of points in the plane, IEEE Trans. Inf. Theory **29**, 551 (1983).

[70] Y. Furukawa, M. Yamamoto, and T. Kuroda, Ellipsometric study of the transition layer on the surface of an ice crystal, J. Cryst. Growth **82**, 665 (1987).

[71] R. R. Gilpin, Wire regelation at low temperatures, J. Colloid Interface Sci. **77**, 435 (1980).

[72] E. Maras, O. Trushin, A. Stukowski, T. Ala-Nissila, and H. Jónsson, Global transition path search for dislocation formation in Ge on Si(001), Comput. Phys. Commun. **205**, 13 (2016).

[73] A. P. Thompson, H. M. Aktulga, R. Berger, D. S. Bolintineanu, W. M. Brown, P. S. Crozier, P. J. in 't Veld, A. Kohlmeyer, S. G. Moore, T. D. Nguyen, R. Shan, M. J. Stevens, J. Tranchida, C. Trott, and S. J. Plimpton, LAMMPS—a flexible simulation tool for particle-based materials modeling at the atomic, meso, and continuum scales, Comput. Phys. Commun. **271**, 108171 (2022).

[74] W. M. Brown, J. Y. Carrillo, N. Gavhane, F. M. Thakkar, and S. J. Plimpton, Optimizing legacy molecular dynamics software with directive-based offload, Comput. Phys. Commun. **195**, 95 (2015).

[75] H. C. Edwards, C. R. Trott, and D. Sunderland, Kokkos: Enabling manycore performance portability through polymorphic memory access patterns, J. Parallel Distrib. Comput. **74**, 3202 (2014).

[76] A. Stukowski, Visualization and analysis of atomistic simulation data with OVITO—the Open Visualization Tool, Modell. Simul. Mater. Sci. Eng. **18**, 15012 (2009).

[77] M. J. Abraham, T. Murtola, R. Schulz, S. Páll, J. C. Smith, B. Hess, and E. Lindahl, GROMACS: High performance molecular simulations through multi-level parallelism from laptops to supercomputers, SoftwareX **1-2**, 19 (2015).

[78] M. J. Shultz, Ice surfaces, Annu. Rev. Phys. Chem. **68**, 285 (2017).

[79] H. Iglev, M. Schmeisser, K. Simeonidis, A. Thaller, and A. Laubereau, Ultrafast superheating and melting of bulk ice, Nature (London) **439**, 183 (2006).

[80] V. I. Kalikmanov, *Nucleation Theory* (Springer, Dordrecht, Netherlands, 2013).

[81] L. Lupi, A. Hudait, B. Peters, M. Grünwald, R. Gotchy Mullen, A. H. Nguyen, and V. Molinero, Role of stacking disorder in ice nucleation, Nature (London) **551**, 218 (2017).

[82] D. Faken and H. Jónsson, Systematic analysis of local atomic structure combined with 3D computer graphics, Comput. Mater. Sci. **2**, 279 (1994).

[83] P. B. Louden and J. D. Gezelter, Friction at ice- I_h /water interfaces is governed by solid/liquid hydrogen-bonding, J. Phys. Chem. C **121**, 26764 (2017).

[84] G. A. Tribello, M. Bonomi, D. Branduardi, C. Camilloni, and G. Bussi, PLUMED 2: New feathers for an old bird, Comput. Phys. Commun. **185**, 604 (2014).

[85] J. R. Errington and P. G. Debenedetti, Relationship between structural order and the anomalies of liquid water, Nature (London) **409**, 318 (2001).